THE JOURNAL OF PHYSICAL CHEMISTRY A

 VOLUME 104, NUMBER 32, AUGUST 17, 2000

ARTICLES

Simulation of a Liquid State Photoinduced Enol-Keto Tautomerization Involving Long-Range Proton Transfer

J. D. Geerlings, C. A. G. O. Varma,* and M. C. van Hemert

Leiden Institute of Chemistry, Leiden University Gorlaeus Laboratories, P.O. Box 9502, 2300 RA Leiden, The Netherlands

Received: February 18, 2000; In Final Form: May 25, 2000

Photoexcited 7-hydroxy-8-(*N*-morpholinomethyl)quinoline (HMMQ) has previously been shown to transform from the excited enol form E* into the excited keto form K* in a number of consecutive elementary processes involving formation of an excited zwitterionic form Z* and rotational Brownian motion of the morpholino group which acts as a proton carrier and gets into motion only if its initial *intra*molecular H-bond is broken thermally. The latter motion is not restricted to cases in which HMMQ is dissolved in polar solvents, but may proceed also in nonpolar media which contain proton accepting solvents such as 1,4-dioxane. Molecular dynamics simulations of the motion of the morpholino group in the forms E and Z* in liquid cyclohexane and in liquid 1,4-dioxane are presented. The simulation of Z* in cyclohexane reveals that an *intra*molecular hydrogen bond between the protonated N atom in the morpholino group and the deprotonated O atom inhibits the rotational motion of the proton carrier during the whole period of simulation. In the case of Z* in 1,4-dioxane, an *inter*molecular H-bond is formed at the expense of the *intra*molecular hydrogen bond and then the protonated carrier drags the solvent molecule along its path in the rotational Brownian motion. The main conclusions are summarized at the end of the publication.

1. Introduction

Reliable predictions concerning the course of chemical reactions in liquid solutions require a full understanding of the interplay between solute and solvent molecules. The most relevant early theory describing liquid-state reactions was given by Kramers.[1,2] It applies to reactions involving a single reaction coordinate and treats the liquid as a continuous medium providing a random force and friction to drive and damp the motion of the reaction coordinate. Kramers' theory gained attention from chemists only after laser spectroscopic studies of liquid-state reactions in the picosecond domain became available. Since then several improvements of the theory have been offered. Molecular descriptions of liquid-state chemical reactions are quite rare.[3−6] The proper choice between continuum and molecular theories can only be made if they are confronted with reactions whose mechanisms and dynamics are known experimentally with great certainty.

A few years ago, the molecule 7-hydroxy-8-(*N*-morpholinomethyl)quinoline (HMMQ)[7] was designed (see Figure 1). It exhibits a photoinduced tautomerization in polar solvents. The mechanism involves first the conversion of the excited enol form E* into a zwitterionic form Z* in which the morpholino group is protonated. The side group delivers the proton at the final destination after motion over a fairly large distance and then the excited keto form K* is formed (see Figure 2). Since proton tunneling through a hydrogen bond is involved in each of the two proton transfer steps, the initial and final conditions are known accurately in the reference frame of the tautomerizing

10.1021/jp000664v CCC: $19.00
Published on Web 07/20/2000

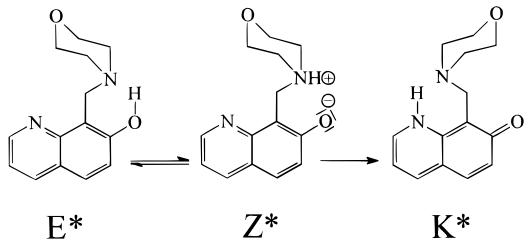

Figure 1. Excited-state intramolecular proton transfer (ESIPT) process in HMMQ.

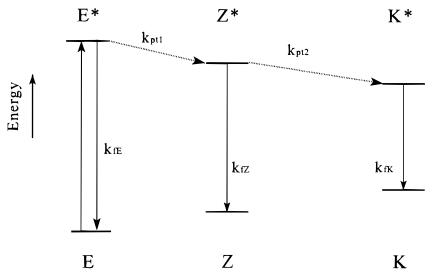

Figure 2. Kinetic scheme for the evolution of E* into K*.

molecule both in space and time. The effects of solvent friction and dielectric permittivity on the motion of the protonated side group has been studied by means of time-resolved fluorescence spectroscopy.[8−10] Several continuum models have been applied to simulate the observed effects of friction.[7] The simulations did not reproduce the observations quite well, perhaps due to imperfections in the friction models or due to unrealistic modeling. At that time there was no experimental indication that the side group could be loaded with an H-bonded solvent molecule which has to be carried along the whole path. This feature, which may have a substantial friction influence, had not been taken into account in the simulations. Now there is experimental evidence for the formation of such a solute−solvent complex in the case of HMMQ in 1,4-dioxane.[11,12] The molecular dynamics (MD) studies presented here serve to extend the understanding of the action of the solvent in the course of the photoinduced enol-keto tautomerization of HMMQ in liquid 1,4-dioxane.

A kinetic scheme for the evolution of E* into K* is shown in Figure 2. The rate constants of the radiative processes involving E*, Z*, and K* are indicated with k_{fE}, k_{fZ}, and k_{fK}, respectively, and the rate constants of the two proton-transfer steps are indicated by k_{pt1} and k_{pt2}. The first proton transfer leading to the formation of Z* is accomplished within less than 10^{-12} s after preparation of E*.[7−11] Since the proton in this tunneling process has an essential quantum mechanical character, the process is not included in the classical MD simulation of HMMQ presented in this paper. A number of mixed quantum/classical MD methods have been developed and applied to proton-transfer reactions in solutions.[13−22] In these methods the hydrogen atom is treated quantum mechanically while the remaining nuclei are treated classically.

In the case of HMMQ in 1,4-dioxane it is quite certain that, after excitation, the proton tunnels through the *intra*molecular H-bond in less than 10^{-12} s, but the action of the solvent in the subsequent rotational Brownian motion of the protonated side group has not been revealed completely. The treatment of the tunneling step in the proton transfer process in HMMQ is beyond the scope of this paper. In contrast with the tunneling steps, the transformation of Z* into K* takes place on a much longer time scale, because the relatively slow rotation of the protonated side group of Z* is rate determining. Note that the proton is now carried by the morpholino side group over a long distance of at least 0.5 nm. The rotation of the protonated side group in Z* is strongly influenced by electrostatic interactions with the solvent and can be described classically. Intriguing questions are how 1,4-dioxane molecules interact with Z* and how the solvent enables the rotation of the side group. To answer these questions, classical MD simulations of the ground state enol form of HMMQ (E) dissolved in 1,4-dioxane are performed first. A specific HMMQ configuration, in which the H atom of the OH group is sufficiently close to the morpholino N atom, is selected for this simulation. Excitation of E in that configuration will then immediately lead to Z* by tunneling of the proton through the *intra*molecular H-bond. The force fields are adapted to the replacement of E by Z* and the MD simulations are continued with HMMQ in the Z* form.

The force field parameters for the solute, HMMQ, are largely taken from the AMBER[23,24] and GROMOS[25] force fields. The aromatic ring system of HMMQ is regarded as a rigid structure because it does not change shape during the proton transfer reaction. The morpholino side group and the OH group are treated in a special way because the main interactions with the solvent during the proton transfer take place at these sites. The site charges of E and Z* are obtained by quantum chemical calculations. In the simulations the excited state character of Z* is expressed by adapting the chosen site charges. The charge distribution in Z* depends on the torsion angles, which vary during the rotation of the positively charged morpholino group. Therefore the site charges in Z* are calculated for a series of configurations with various positions of the side group with respect to the quinoline ring. The interaction potential of 1,4-dioxane, presented in a previous paper[26] dealing with MD simulations of a dipole in liquid dioxanes, is used for the MD simulation of HMMQ in liquid 1,4-dioxane. This paper shows that the use of an Ewald summation of electrostatic terms instead of a cutoff radius in the simulation does not lead to a substantial modification of the reaction field experienced by the dipole, because this field arises predominantly from partial dipoles of its nearest dioxane neighbors. With this in mind, the time-consuming Ewald summation is not used in the present simulations.

From fluorescence experiments it is concluded that the long distance proton-transfer process in HMMQ does not take place in cyclohexane, because there is no evidence for fluorescence of K* in this solvent, in contradiction to the case of HMMQ in 1,4-dioxane.[7−11] So, in addition simulations of HMMQ in cyclohexane are performed to verify that the MD calculations can correctly predict the presence or absence of long-range proton transfer.

2. Quantum Chemical Molecular Calculations

A number of molecular properties, needed to create force fields for the MD calculations, have been calculated with ab initio quantum chemical methods. The large size of HMMQ imposes limitations on the level of sophistication of these calculations. A straightforward optimization of the geometry of HMMQ has not been feasible. Instead, an optimal geometry of HMMQ has been determined by composing an initial structure based on fragments HYMEQ (Figure 4a) and MMORPH (Figure 4b), whose geometries had been optimized with SCF calculations, and optimization of the newly introduced degrees of freedom at the SCF level. The excited states of the species have been obtained with open shell SCF calculations, using a double-ζ (DZ) basis. Comparison of DZ-basis-open shell SCF and CI results for the fragments justifies the use of excitation

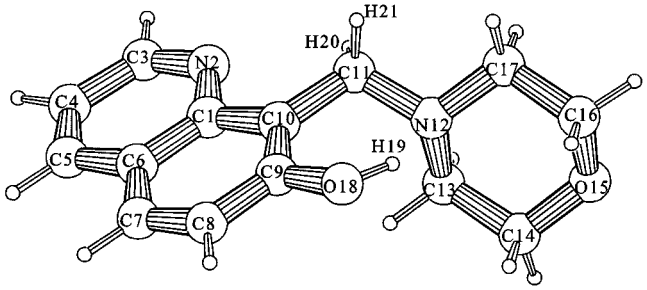

Figure 3. Geometry of the enol form of HMMQ in the ground state, obtained from SCF calculations.

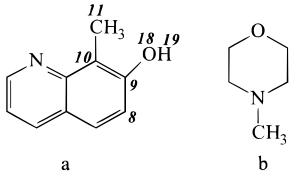

Figure 4. Molecules related to HMMQ: (a) HYMEQ; (b) MMORPH.

TABLE 1: Lennard-Jones Site Parameters for HMMQ

(united) atom site S	σ_S/nm	ϵ_S/kJ mol^{-1}
C1,C3−C10, N12	0.370	0.502
N2	0.350	0.669
N12	0.385	0.502
O15, O18	0.330	0.628
H19	0.200	0.084

TABLE 2: Acronyms Referring to the Different Species

compound	acronyms
7-hydroxy-8-(*N*-morpholinomethyl)quinoline	HMMQ
enol form of HMMQ	E
excited state of E	E*
zwitterionic form of HMMQ	Z
excited state of Z	Z*
keto form of HMMQ	K
excited state of K	K*
deprotonated HMMQ	HMMQn
Excited state of HMMQn	HMMQn*
7-hydroxyquinoline	7HQ
7-hydroxy-8-methylquinoline	HYMEQ
excited state of HYMEQ	HYMEQ*
deprotonated HYMEQ	HYMEQn
excited state of HYMEQn	HYMEQn*
N-methylmorpholine	MMORPH
N-ethylmorpholine	EMORPH

energies and charge distributions from the former calculation. The program package Gamess UK[27] has been used for the ab initio quantum chemical calculations. The acronyms referring to different species are presented in Table 2.

The ground-state structure, obtained after optimization of the geometry of HYMEQ, has been used as the model of the aromatic system in HMMQ. The optimal ground-state geometry of MMORPH has been taken as the model for the morpholino side group in the enol form of HMMQ (E in Figure 3). The labels indicated in Figures 3 and 4 are used to refer to the different sites in the molecules. Further optimization of the geometry of E has been achieved by optimizing the bonds which connect the aromatic system to the morpholino group (C10−C11, C11−N12, C11−H20, and C11−H21), the angles between these atoms (C1−C10−C11, C10−C11−N12, C11−N12−C13, and C10−C11−H20/21), and the dihedral angles which define the orientation of the side group with respect to the aromatic system (ϕ_1 = C9−C10−C11−N12, ϕ_2 = C10−C11−N12−C13 and C9−C10−C11−H20/21). Dihedral angles have a value of zero when their four defining atoms are located in a planar cis-configuration. The geometry of the OH group has been determined by optimizing the O18−H19 bond, the angles C9−O18−H19 and C8−C9−O18, and the dihedral angle ϕ_3 = C8−C9−O18−H19. The structure of HMMQ in the enol form, shown in Figure 4, is the final result from the SCF calculations. The aromatic system is flat and the ring of the side group is oriented almost perpendicular to the aromatic ring system. In the equilibrium structure the N atom of the morpholino group lies below the plane of the aromatic ring system and points toward the OH group; this corresponds to a rotation (ϕ_1) around the C10−C11 bond of 41 degrees. The morpholino group is rotated around the C11−N12 bond such that the lone pair of N12 is directed toward H19, which corresponds to a value of 200 degrees for ϕ_2. The distance between O18 and N12 is 0.273 nm and the distance between H19 and N12 amounts to 0.193 nm. The latter distance is short enough to consider the link as a H-bond. This result applies to the ground state of isolated HMMQ. The proton in the *intra*molecular H-bond is not located on the line connecting the proton donor O18 and the acceptor N12. This is clearly seen in Figure 3.

TABLE 3: Differences Between SCF Energies

species 1	species 2	$E_1 - E_2$[a]/kJ mol^{-1}
E*	E	348[b]
Z	E	185
Z*	E	474
HMMQn	E	1583
HMMQn*	E	1762
HYMEQ*	HYMEQ	347[b]
HYMEQn	HYMEQ	1514[c]
HYMEQn*	HYMEQ	1702
$EMORPHH^+$	EMORPH	−767[d]
1,4-dioxane-H^+	1,4-dioxane	−845[d]

[a] E_1 and E_2 are the SCF energies of species 1 and 2, respectively [b] $S_0 - S_1$ excitation energy of E. [c] Deprotonation energy (E_D) i.e., energy required to abstract the proton from the OH group of the molecule in a vacuum. [d] Protonation energy (E_P) i.e., energy gained in the protonation of the molecule in a vacuum.

The optimized geometry of Z* at the SCF level is obtained by introducing the optimized structures of HYMEQn* and of MMORPH as fixed structures in Z*. The Z* structure is then further optimized by variation of the remaining degrees of freedom, namely the bond angles C10−C11−N12, C10−C11−H20, C10−C11−H21, and the dihedral angles ϕ_1, ϕ_2, C9−C10−C11−H20, and C9−C10−C11−H21.

Table 3 summarizes the differences in SCF energy (DE_{SCF}) among the various states emerging from HMMQ and HYMEQ. The calculated wavelength of the first UV/visible transition in both HYMEQ and HMMQ amounts to 344 nm, which is close to the first band (330 nm) in the absorption spectrum of both HMMQ and 7-hydroxyquinoline (7HQ).

The SCF gas-phase deprotonation energies (E_D) of HMMQ and HYMEQ amount to 1583 and 1514 kJ mol^{-1}, respectively. In the case of HMMQ* and HYMEQ* the SCF values of E_D are equal to 1414 and 1450 kJ mol^{-1}, respectively. This confirms the experimentally based conclusion that less energy is required for deprotonation in the excited state than in the ground state. The SCF protonation energies (E_P) of EMORPH and 1,4-dioxane are also given in Table 3. Transfer of the proton from the OH group in E or E* to 1,4-dioxane is energetically more favorable by an amount of 78 kJ mol^{-1} than to EMORPH. In other words 1,4-dioxane can be protonated in the gas phase by E*.

The results from the open shell SCF calculations may be considered sufficiently accurate if extension with CI does not affect the energy differences appreciably. The table CI option

TABLE 4: Excitation Energy, Oscillator Strength, and Lifetime of the $S_0 - S_1$ Transition of HYMEQ and HYMEQn from the CI Calculation with DZ Basis

energy/kJ mol^{-1}	symmetry	oscillator strength f	radiative lifetime τ_r/ns
		HYMEQ	
379	A′	0.043	30
516	A′	0.066	12
609	A′		
496	A″	6.2×10^{-3}	131
606	A″	0.047×10^{-3}	12×10^3
713	A″		
770	A″		
		HYMEQn	
290	A′	0.13	19
384	A′	0.39	33
670	A′		
393	A″	0.012×10^{-3}	0.11×10^6
488	A″	0.084×10^{-3}	10×10^3
496	A″		
588	A″		

in the Gamess package has been used for the CI calculation of the states of HYMEQ and HYMEQn. In a series of steps the set of reference configurations for a system with 22 active electrons and 74 molecular orbitals has been optimized. The final set consists typically of 40 configurations. Single and double excitation with respect to this reference set leads to a configuration space of roughly 10^7 SAFs (symmetry adapted functions) of which 10 000 have been selected for final diagonalization. In the CI calculations of HYMEQn, two additional electrons, i.e., a total of 24 active electrons, have been taken into account, because the lowest two active molecular orbitals are nearly degenerate.

The deprotonation energy at the CI level amounts to 1433 kJ mol^{-1}, slightly lower than the SCF value of 1514 kJ mol^{-1} found previously. The energies of the excited states reached by (optical) excitation from the ground state are presented for both molecules in Table 4. For some states also the oscillator strength f and the radiative lifetime τ are included. The excitation energy of the first excited state of HYMEQ with A′ symmetry corresponds to a wavelength of 315 nm, which is close to where it is expected but somewhat below the wavelength predicted by the SCF calculations. The second excited state from the CI is also of A′ symmetry and has an excitation energy corresponding to a wavelength of 231 nm. Since this transition has a large oscillator strength it can be identified with the strong band observed in the region between 200 and 300 nm in the absorption spectrum of HMMQ and 7HQ. The deprotonation energy of HYMEQ in the excited-state amounts to 1331 kJ mol^{-1}.

The scheme in Figure 5 shows the CI energy differences and the SCF energy differences between states of HYMEQ and HYMEQn. Both types of calculation show a large energy gap between the ground state of HYMEQ and the ground state of HYMEQn, and also between their excited states. The calculated deprotonation energy E_D of HYMEQ (or HMMQ) is reduced in going from the ground state to the first excited singlet state. However, the energy loss after deprotonation of HYMEQ (or HMMQ) in the excited state can also not be fully compensated by the energy gained in the acceptance of the proton by a 1,4-dioxane molecule or, in the case of HMMQ, by the morpholino side group. This means that in the case of HMMQ, external energy has to be added to transfer the proton *intra*molecularly from the OH group to the N atom in the morpholino side group in the isolated excited molecule. Solvation is required for the stabilization of the excited zwitterionic form. The solvent must

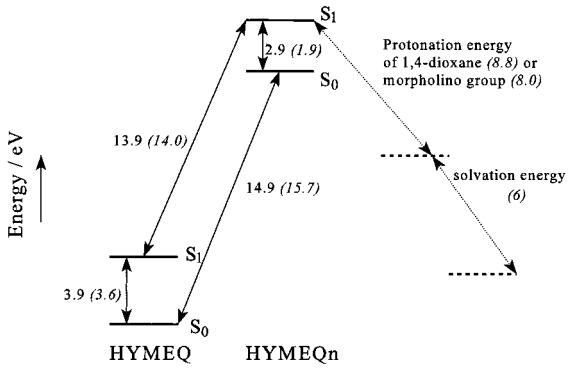

Figure 5. State energies (in eV) of HYMEQ and deprotonated HYMEQ (HYMEQn) from SCF (between brackets) and from CI calculations with a DZ basis.

stabilize the molecules in such a way that an additional energy of more than 530 kJ mol^{-1} is gained. Since a typical value of the solvation energy of an inorganic ion pair in water is about 750 kJ mol^{-1},[28] it is likely that a solvation energy of at least 530 kJ mol^{-1} can be obtained upon formation of the protonated morpholino group from excited HMMQ.

The dihedral angles ϕ_1 and ϕ_2 are the most important variables needed to describe the rotation of the side group in HMMQ. The potential for this motion has been calculated as a function of ϕ_1 and ϕ_2 in the SCF approximation with DZ basis (SCF surface). Both dihedral angles have been changed in steps of 30 degrees. The SCF surface of E is plotted as a function of ϕ_1 and ϕ_2 in Figure 6a. The plot shows that the barrier to be crossed during the rotation is very large when either one of the variables is kept fixed. Only simultaneous variations in ϕ_1 and ϕ_2 can result in a relatively low energy path for the rotation of the morpholino group. The CH_2 groups (C13, C14) in the morpholino group are sterically hindered by the OH group and by the N atom in the quinoline ring. The saddle point at $(\phi_1,\phi_2) = (180°,240°)$ corresponds to the configuration of E, in which N12 is close to N2. The barrier at this point is about 100 kJ above the minimum. The parts in the surface in Figure 6a to the left and to the right of $\phi_1 = 180°$ correspond to the conformations of E, in which the morpholino side group is either above or below the plane of the quinoline ring. They are not mirror images of each other, because the OH group is not coplanar with the quinoline skeleton in the equilibrium structure of E. The OH bond points either below or above the plane of the quinoline skeleton.

To determine the SCF energy for the H-bond between N12 and H19 additional SCF calculations have been performed in which the value of ϕ_3 is changed from 161° (the optimal value for H-bonding) to −20°. The N12−H19 distance increases from 0.193 to 0.368 nm in the latter geometry, which means that the H-bond does not exist anymore. The increase in SCF energy of the system is then 63 kJ mol^{-1}. This energy is decreased by an amount of 28 kJ mol^{-1}, after optimization of the limited number of degrees of freedom, which had also been taken into account in the optimization of the geometry of E, with the exception of ϕ_3. In other words the decrease in energy is caused by removal of the strain of the pseudo ring (constructed by the sites N12, C11, C10, C9, O18, and H19). In this approach the SCF binding energy thus amounts to 37 kJ mol^{-1}, which is slightly larger than expected (ca. 25 kJ mol^{-1}).[29] For fitting purposes further SCF calculations are performed where the N12−H19 distance is changed by small amounts through small variations of ϕ_1, ϕ_2 and ϕ_3 around their equilibrium values.

The open shell SCF surface for Z* is shown in Figure 6b as a function of ϕ_1 and ϕ_2. It shows that the potential wells on the

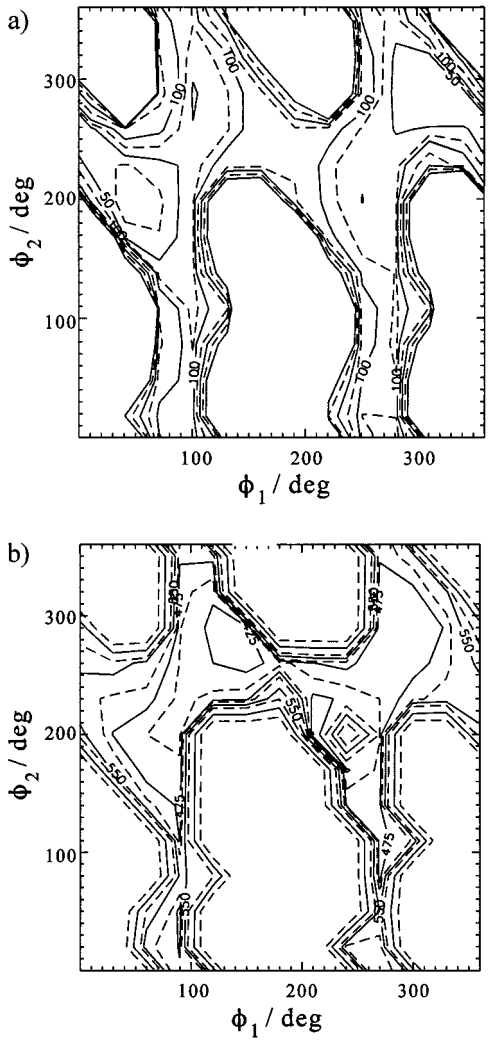

Figure 6. Potential energy surfaces as a function of ϕ_1 and ϕ_2 and with energy in kJ mol^{-1}, from SCF calculations with DZ basis, for different forms of HMMQ: (a) the ground-state enol form E; (b) the excited zwitterionic form Z*.

Z* surface are shifted with respect to their location on the SCF surface for E. They correspond to conformations of Z* in which the formation of an *intra*molecular H-bond between H19 and N2 is enabled.

3. Force Fields

Several force fields are required in the MD calculations, namely the *intra*molecular force field for the ground state of the enol form (E) and the excited state (Z*) of the zwitterionic form of HMMQ, the force fields for the solvents 1,4-dioxane and cyclohexane and the force fields for the solute−solvent and solvent−solvent interactions. Most of the force field parameters needed could be obtained from the literature. The missing parameters have been derived from the results of the quantum chemical calculations.

The most important feature in the dynamics of HMMQ concerns the motion of the two ring systems with respect to each other. Only small angular distortions of the rings are allowed, while their bond lengths are kept constant. The potential energy of the molecule, either in the E state or in the Z* state, is written as a sum over harmonic potentials for covalent bond stretching, for bond-angle bending, for improper dihedral-angle bending, for dihedral-angle torsion, and an additional sum over the Lennard-Jones and Coulomb potentials for the nonbonded interactions between sites:

$$U_{\text{pot}} = \sum_{l=1}^{N_b} \frac{R_l}{2}(b_l - b_{0l})^2 + \sum_{l=1}^{N_\theta} \frac{T_l}{2}(\theta_l - \theta_{0l})^2 + \sum_{l=1}^{N_\xi} \frac{G_l}{2}(\xi_l - \xi_{0l})^2 + \sum_{l=1}^{N_\phi} \frac{V_l}{2}[1 + \cos(n_l\phi_l - \delta_l)] + \sum_{i}^{N_{at}} \sum_{j>i}^{N_{at}} \left[\frac{A_{ij}}{r_{ij}^{12}} - \frac{B_{ij}}{r_{ij}^{6}} + \frac{q_i q_j e^2}{4\pi\epsilon_0 r_{ij}} \right] \quad (1)$$

where R_l, T_l, and G_l are the force constants for the harmonic oscillations of the bond length b_l, the bond angle θ_l, and the improper (GROMOS terminology) dihedral angle ξ_l, respectively. The force field parameters for the torsional dihedral angles are the force constant V_l, the multiplicity n_l, the dihedral angle ϕ_l, and the phase shift δ_l. The parameters of the Lennard-Jones potential are denoted as A_{ij} and B_{ij}, and the charges on site i and site j with a distance of r_{ij} between them are denoted as q_i and q_j, respectively.

The parameters R_l and T_l are taken from the AMBER force field.[24] The summation in the third term includes only dihedral angles which are selected to keep atoms close to a specific spatial configuration. In the fourth term the summation includes those dihedral angles needed to describe the hindered rotation of a particular group of atoms. The simulations of HMMQ (see Figure 3) allow rotation around the C11−N12 bond (morpholino group), around the C10−C11 bond (CH_2 group) and around the C9−O18 bond (OH group). These rotations thus involve the torsional dihedral angles ϕ_1 = C9−C10−C11−N12, ϕ_2 = C10−C11−N12−C13, and ϕ_3 = C10−C9−O18−H19, respectively. The other dihedral angles are treated as being improper. The force constants G_l are taken from the GROMOS force field and the V_l values from the AMBER force field. The equilibrium values b_{0l}, θ_{0l}, and ξ_{0l} are derived from ab initio SCF calculations.

The parameters A_{ii} and B_{ii} in the Lennard-Jones potential have been calculated from the well depth parameter ϵ_i and the van der Waals diameter σ_i of atom i by applying $A_{ii} = 4\epsilon_i\sigma_i^{12}$ and $B_{ii} = 4\epsilon_i\sigma_i^{6}$. The parameters ϵ_i and σ_i for sites in HMMQ are from the AMBER force field (Table 1). The values of A_{ij} and B_{ij} are the geometric averages $A_{ij} \equiv (A_{ii}\times A_{jj})^{1/2}$ and $B_{ij} \equiv (B_{ii}\times B_{jj})^{1/2}$. The Lennard-Jones interactions between two atoms, which are three bonds away from each other or which are members of the same ring, have been reduced by 50%. The Lennard-Jones and Coulomb interactions between neighbor atoms and second neighbor atoms are not taken into account, these atoms are referred to as, in GROMOS terminology, excluded neighbors.

Mulliken atomic charges (Q_M) from the SCF calculation with the DZ basis have been used as a reasonable first approximation for the atomic charges, because a Mulliken population analysis in the CI calculation of HMMQ with the DZ basis was not feasible. The site charges q_i have been obtained by proper scaling of the Mulliken charges and subsequent summation of the scaled charges belonging to the specific site when this is treated as a united atom (Table 5). The scaling factor is 0.67, equal to the factor which was found to be suitable for the charges in pure 1,4-dioxane.[26] The CH and CH_2 groups are treated as united atom sites.

To let the force field (FF) surface resemble the SCF surface closely, some parameters from the AMBER force field[24] have been adjusted. For the purpose of calculating H-bond energies, the usual r^{-6} attractive term in the Lennard-Jones potential has

TABLE 5: Site Charges in Different Forms of HMMQ, Derived from the Scaled Mulliken Atomic Charges of the SCF Calculations with DZ Basis (unit = |electron charge|)

atom	E	HMMQn*	Z	Z*
C1	−0.009	−0.024	+0.013	−0.008
N2	−0.237	−0.338	−0.314	−0.400
C3	−0.043	−0.179	−0.010	−0.081
C4	+0.0133	−0.062	−0.006	+0.002
C5	−0.007	−0.249	−0.016	−0.209
C6	+0.310	+0.347	+0.311	+0.402
C7	−0.140	−0.237	−0.151	−0.243
C8	−0.122	−0.215	−0.167	−0.096
C9	+0.273	+0.160	+0.300	+0.070
C10	+0.160	+0.154	+0.064	+0.179
C11	+0.163	+0.118	+0.214	+0.228
N12	−0.513	−0.404	−0.626	−0.646
C13	+0.179	+0.146	+0.279	+0.299
C14	+0.216	+0.189	+0.237	+0.239
O15	−0.499	−0.519	−0.483	−0.474
C16	+0.224	+0.199	+0.268	+0.272
C17	+0.201	+0.181	+0.349	+0.377
O18	−0.646	−0.265	−0.747	−0.368
H19	+0.476		+0.485	+0.458

been replaced by an r^{-10} term in the AMBER force field. Since this modification cannot be included easily in the GROMOS program package, the parameters ϵ_{ij} and σ_{ij} for the interaction between N12 and H19 have been adjusted to reproduce the SCF energy of the *intra*molecular H-bond. The value of σ_{ij} has been chosen such that the N12−H19 equilibrium distance is close to the SCF equilibrium distance. This value turns out to be equal to the value of σ_{ij} for N−H and O−H hydrogen bonds in the AMBER force field (0.178 nm).[24] The value of ϵ_{ij} has been determined by constructing potential energy surfaces as a function of ϕ_1, ϕ_2 and ϕ_3 for various trial values. Surfaces with a single minimum could only be obtained by adjusting the value of V_3 also. The final values of ϵ_{ij} and V_3 are 41.8 kJ mol^{-1} and 2.5 kJ mol^{-1} and yield an energy of 24 kJ mol^{-1} for the H-bond.

The FF surface obtained with the adjusted parameters is shown in Figure 7a as a function of ϕ_1 and ϕ_2. It resembles the SCF surface, but the barrier at the saddle point $((\phi_1,\phi_2) = (180,250)$ is much (ca. 300 kJ) higher. This difference is not of any concern, because the barrier is too high in both cases for thermal barrier crossing at 300 K. On the FF surface another high barrier appears, at $(\phi_1,\phi_2) = (0,200)$, which is not encountered on the SCF surface. It arises mainly from the large repulsion in the Lennard-Jones potential, when N12 is the vicinity of O18 and H19. When only ϕ_1 and ϕ_2 are varied, distances between atom pairs are encountered which are slightly shorter than their van der Waals distance. This imperfection disappears in the MD simulation, because the other degrees of freedom are then not fixed.

In the FF for Z* the values of the Lennard-Jones parameters for the pairs H19−O18 and H19−N2 have been set equal to the values used for the H19−N12 pair in E. Two different force fields for Z* have been used. In the first one the site charges for the optimal geometry of Z* are used and kept fixed. In the second one a number of selected sites in Z* have charges which are considered to be functions of ϕ_1. These are the sites whose charge varies significantly, when the value of ϕ_1 is changed in the SCF calculations. The only site whose charge is modified significantly upon variation of ϕ_2 is O18, namely when H19 is close to O18. Therefore ϕ_2 is kept fixed and its value is set at 260°, because only then could convergence be obtained for all the chosen values of ϕ_1 in the open shell SCF calculations. The set of selected sites in Z* consists of C1, N2, C13, C17, O18, and H19. A continuous function of ϕ_1 is fitted to the calculated

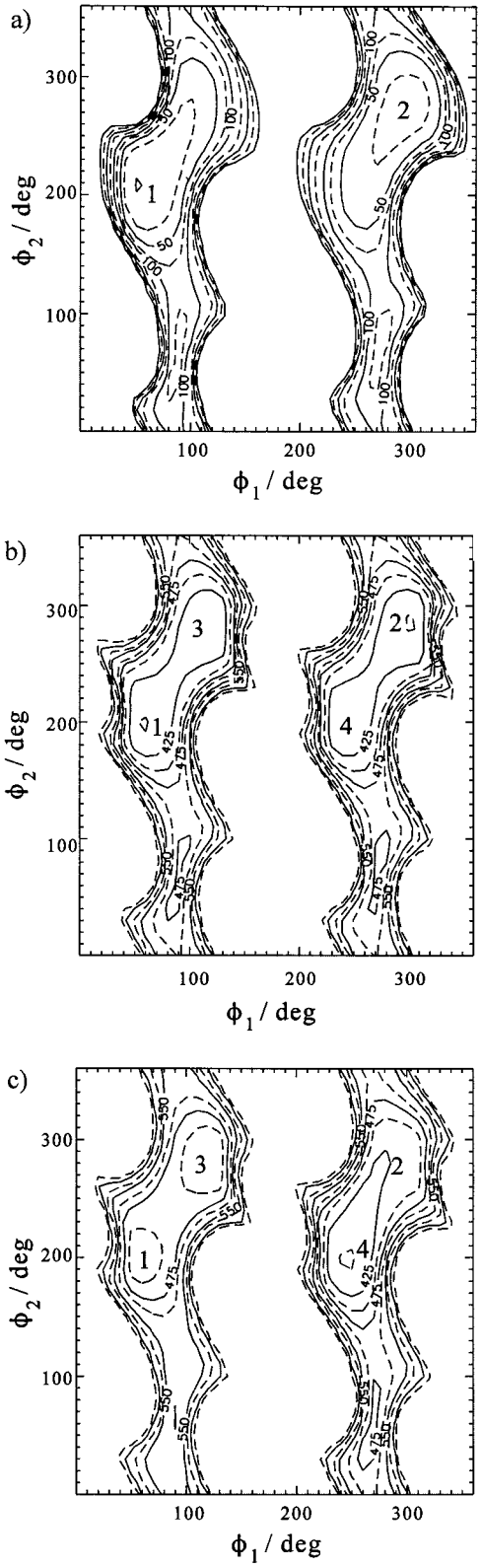

Figure 7. Potential energy surfaces as a function of ϕ_1 and ϕ_2 and with energy in kJ mol^{-1}, resulting from force field U_{IJ} for different forms of HMMQ: (a) the ground-state enol form E; (b) the excited zwitterionic form Z* and force field with fixed charges for the optimized geometry of Z*; (c) excited zwitterionic form Z* and force field with site charges of Z* depending on ϕ_1.

charge for each member in the set. The charge on O18 is represented by a Gaussian function of ϕ_1. The charges on C1, N2, C13, C17, and H19 are represented by sine functions of ϕ_1. The calculated and fitted site charges are shown in Figure

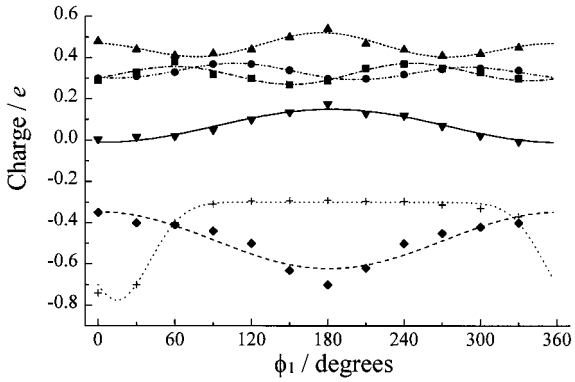

Figure 8. Site charges in Z* as a function of ϕ_1. The symbols ▼, ◆, ■, ●, +, and ▲ present the site charges on C1, N2, C13, C17, O18, and H19 derived from Mulliken SCF (DZ basis) atomic charges. Lines represent the fitted functions.

8. The calculated total charge (Q_{tot}) of Z* is not always equal to zero. When this occurs, a value of $-Q_{tot}/19$ is added to each site charge. The largest correction (± 0.03) is required when the charge on O18 is minimal. Because site charges are kept fixed during MD simulations with the standard GROMOS package, a routine for the modification of the site charges as functions of ϕ_1 has been introduced in the package. The first force field yields the FF surface shown in Figure 7b. This has four energy wells (1−4) of which two (1 and 2) correspond to the configuration of Z* having an *intra*molecular H-bond between H19 and O18 and the other two (3 and 4) correspond to the configuration of Z* with an *intra*molecular H-bond between H19 and N2. The FF surface resulting from the second force field is shown in Figure 7c. The energy wells 3 and 4 are now deeper than the wells 1 and 2. This implies that the configuration of Z*, which enables the formation of K*, is energetically slightly more favorable. Differences between the *intra*molecular force fields for E and Z* arise mainly from the differences in their site charges. Smaller differences arise from the differences in optimized geometries of E and Z*.

The solvent−solvent and solute−solvent interactions have been calculated as a sum over the Coulomb and the Lennard-Jones *inter*molecular site interactions as described previously[26] with parameters A_{ij} and B_{ij} for interaction of sites of different type taken, as in the case of the *intra*molecular force field, as $A_{ij} \equiv (A_{ii} \times A_{jj})^{1/2}$ and $B_{ij} \equiv (B_{ii} \times B_{jj})^{1/2}$. However, this is not suitable for the calculation of the energy of the *inter*molecular H-bond in the case of HMMQ dissolved in 1,4-dioxane. Then values of ϵ and σ for the O_{diox}−H19 interaction are taken which are also used for the *intra*molecular H-bond of HMMQ. The site charges on the O atoms (O_{diox}) and the CH_2 groups of 1,4-dioxane are $-0.35e$ and $+0.175e$, respectively, and the molecule is kept rigid in the optimal chair geometry during the MD simulation. The values of the parameters ϵ_i and σ_i for the CH_2 group of 1,4-dioxane are 59.4 K and 0.3905 nm, respectively, and for its O atoms the values of these parameters are 85.6 K and 0.3070 nm, respectively. The geometry of cyclohexane, used in the simulation, is a chair conformation which has been optimized at the SCF level. The Lennard-Jones parameters for the CH_2 groups in cyclohexane have been set equal to those for 1,4-dioxane. The site charges in cyclohexane are zero.

4. MD Simulations of HMMQ in 1,4-Dioxane and in Cyclohexane

Periodic boundary conditions are imposed on the system in the MD simulations. All interactions are neglected when the interacting sites are separated by a distance larger than a selected cutoff radius R_c. As usual, R_c is set equal to 0.5 L, where L is the length of the initial (cubical) box. Rigidity of the molecules is maintained by applying the SHAKE coordinate resetting procedure.[30] All calculations have been performed on nodes of the local IBM SP computer. Ensembles with constant number of molecules (N), constant pressure (P), and constant T (NPT ensemble) with $P = 1$ atm, $T = 298$ K are used. Pressure and temperature of the solvent are controlled during the simulation by using the velocity and position scaling method of Berendsen et al.[31] at each time step. The method mimics the relaxation of the solvent coupled to a bath at constant temperature (T) or pressure (P), by introducing time constants τ_T and τ_P to achieve constant temperature and pressure, respectively. The equilibration starts with an initial Maxwell distribution at 298 K for the velocities of the solvent molecules and provides for strong coupling to the bath by taking $\tau_T = 0.01$ ps and $\tau_P = 0.01$ ps. The velocities of HMMQ are not scaled. The kinetic energy of HMMQ is thus controlled only by the interactions of HMMQ with the solvent molecules. The time step dt and the cutoff radius R_c are set at 0.002 ps and 1.30 nm, respectively. A random distribution of initial positions and velocities for the simulation is generated by equilibrating the cubic box with molecules during a period of 100 ps at constant temperature and volume. During the simulations involving the E form of HMMQ, the distances N12−O18, N12−H19, and N2−N12, and the values of ϕ_1, ϕ_2, and ϕ_3 are determined at 20 fs intervals. In the case of the Z* form of HMMQ the distances O18−H19, N12−O18, N2−H19, and N2−N12, and the values of ϕ_1 and ϕ_2 are determined at time intervals of 20 fs. Simulations of systems containing either E or Z* span 600 and 400 ps, respectively. For these simulations $\tau_T = 0.1$ ps and $\tau_P = 0.2$ ps. The positions and velocities of all atoms are collected at every time step.

The simulation box for the solution of HMMQ in liquid 1,4-dioxane is generated in the same manner as in the recent MD study of a dipolar molecular probe in liquid 1,4-dioxane.[26] The box is generated in two steps. First, a single HMMQ molecule is introduced at a random position in the equilibrated cubic box which had been used to start the MD simulation of pure liquid 1,4-dioxane. This box contains 128 dioxane molecules (L = 2.629 nm). After equilibration, all 1,4-dioxane molecules are removed which are separated from HMMQ with *inter*molecular site distances of less than 0.15 nm. The resulting box contains one HMMQ molecule embedded in 125 dioxane molecules.

The procedure applied to obtain the simulation box for the solution of HMMQ in liquid cyclohexane is similar to the one used for the solution in 1,4-dioxane, but in this case the pure liquid solvent had to be simulated first. A cubic box with 125 cyclohexane molecules is created by starting with a single molecule and replicating it in a sequence of 5 translations along three orthogonal directions, with the constraint that the density of the box is equal to that of liquid cyclohexane (0.7791 g/cm^3). Then the box is equilibrated at constant temperature (298 K) and volume during 200 ps and subsequently it is allowed to equilibrate at constant pressure (1 atm) for 40 ps. The resulting box serves as the start of an NPT simulation of liquid cyclohexane for a period of 100 ps. The self-diffusion coefficient (D_l) has been calculated, as described previously for dioxane,[26] and used to verify the adequacy of the force field. The calculated and experimental values of D_l are 3.8×10^{-9} m^2 s^{-1} and 1.4×10^{-9} m^2 s^{-1},[32] respectively. The relative deviation between these values is quite common for MD simulations.[26,33] During the simulations the density of the box remains within 1% equal to that of liquid cyclohexane. The simulation box for the solution

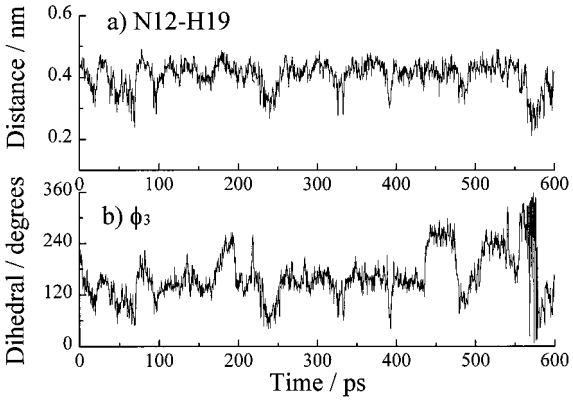

Figure 9. Time dependence (a) of the N12−H19 distance and (b) of ϕ_3, during the simulation of E in 1,4-dioxane.

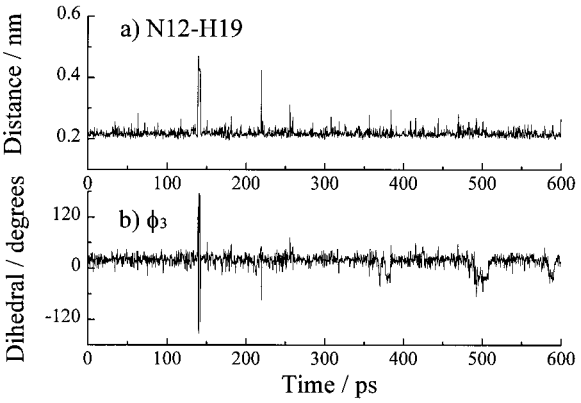

Figure 10. Time dependence (a) of the N12−H19 distance and (b) of ϕ_3 during the simulation of E in cyclohexane.

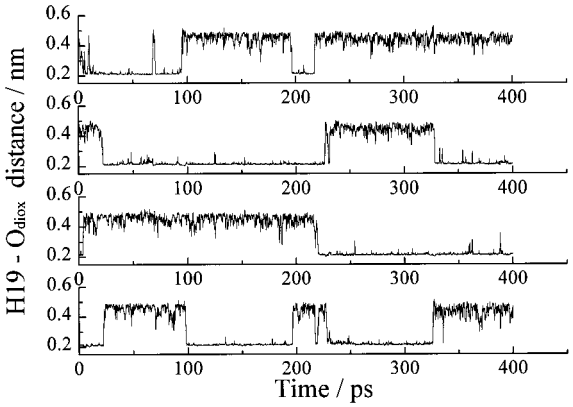

Figure 11. Time evolution of the H19−O_{diox} distances of the four nearest neighbors of species E.

of HMMQ in cyclohexane is obtained by insertion of a HMMQ molecule in the equilibrated box for pure liquid cyclohexane followed by equilibration and subsequent removal of some cyclohexane molecules, which are separated from HMMQ with *inter*molecular site distances of less than 0.17 nm. The box contains then a single HMMQ molecule and 121 cyclohexane molecules.

The simulation of the photoinduced process in which a proton is transferred over the large distance between atoms O18 and N2 (Figure 3) requires two consecutive MD runs. In the first MD run HMMQ is in its electronic ground state (E) and the conformation of E is monitored with intervals of 20 fs to see whether it is suitable for proton tunneling along the *intra*-molecular H-bond between H19 and N12. Conditions to be satisfied then are that the H19−N12 distance should be shorter than 0.25 nm and that the line through H19 and N12 should be nearly perpendicular to the plane through C11, C17, and C13 (with a deviation of less than 15 degrees). The assumption is made that Z* is formed directly from HMMQ by photoexcitation when these conditions are met. Then the second run is started for the actual MD simulation of the solution in which HMMQ is replaced by its Z* form. In this run the following sequence of actions are performed first:

1. The coordinates of H19 in HMMQ are changed such that a bond is formed between N12 and H19.

2. The velocity of H19 is set equal to the velocity of N12.

3. The *intra*molecular force field of E is replaced by the *intra*molecular force field of Z*.

4. The *inter*molecular force field is adapted for the interactions of Z* with the solvent molecules.

The configuration of Z* resulting after these steps is then used to initiate the further evolution of the system. This is investigated in two different manners, namely keeping the site charges in Z* fixed or allowing them to change as the system evolves.

5. Results and Discussion

Figure 9 shows how the N12−H19 distance and the value of ϕ_3 vary as a function of time in the case of the E form in liquid 1,4-dioxane. Most of the time the distance between H19 and N12 is longer than 0.3 nm, while ϕ_3 fluctuates over the whole range of values between 0° and 360°. This implies that the *intra*molecular H-bond between H19 and N12 is then broken. Later on it will become clear that an *inter*molecular H-bond between H19 and an O atom of a 1,4-dioxane molecule exists at this stage. In contrast to this behavior, the E form of HMMQ in cyclohexane retains the *intra*molecular H-bond during the whole simulation period. This can be seen clearly in Figure 10, which presents the time dependence of the N12−H19 distance and of ϕ_3 in the latter case. Changes in ϕ_1, ϕ_2, and ϕ_3 are coupled in such a manner that the *intra*molecular H-bond is not destroyed, apparently because there is no strong interaction between E and cyclohexane molecules. The dihedral angles ϕ_1 and ϕ_2 fluctuate less than in the case of E in 1,4-dioxane. In both solvents the time averaged values of ϕ_1 and ϕ_2, namely $\phi_1 = -60°$, $\phi_2 = -80°$, correspond with energy well 2 at the top right-hand corner of Figure 6b.

Further details of the dynamics of the system with E in 1,4-dioxane are obtained by monitoring at each time step which O_{diox} atoms are nearest to H19. It appears that, most of the time, two O_{diox} atoms are within a distance of about 0.2 nm from H19. This distance is about the length of an H-bond. The next nearest neighbor O_{diox} atoms are at a distance of ca. 0.45 nm. Continuously, molecules at a short distance are moving further away from H19, and vice versa. In Figure 11 the trajectories of the four nearest O_{diox} atoms are represented by a plot of the O_{diox}−H19 distance as a function of time. When a solvent molecule has an O_{diox}−H19 distance of say 0.4 nm at a particular time, it can later be found either at about the same distance, at a shorter distance, or at a longer distance. In the latter case, it does not belong to the set of four nearest neighbors anymore, but is replaced by another solvent molecule, which had a longer O_{diox}−H19 distance previously. This exchange of O_{diox} atoms in the first solvation shell with those in the bulk cannot be seen in Figure 11. A jump in a trace in Figure 11 from 0.2 to 0.4 nm indicates an exchange event in which an O_{diox} atom, which is H-bonded to H19, is exchanged with an O_{diox} in the first solvation shell. Figure 11 shows that an O_{diox} atom dwells

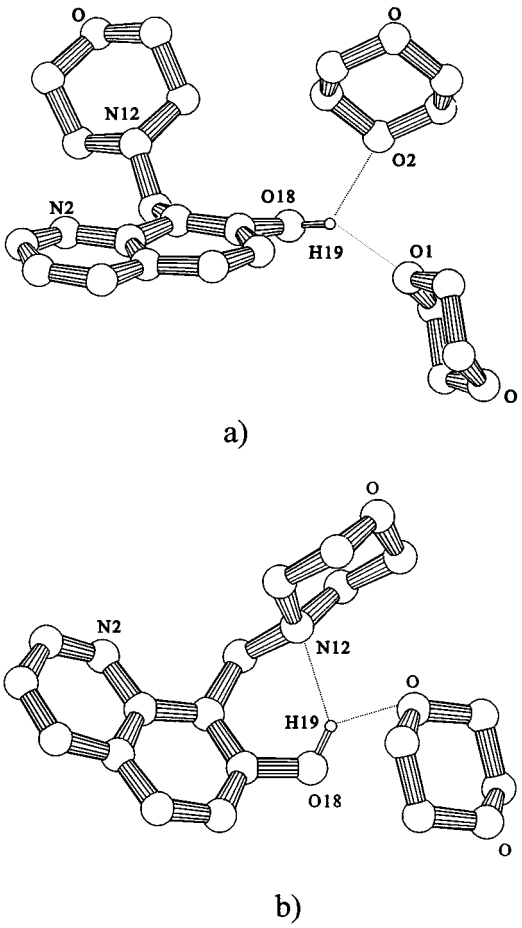

Figure 12. Configurations of E with neighboring 1,4-dioxane molecules: (a) E without intramolecular H-bond and with two 1,4-dioxane molecules at short distance; (b) E with an intramolecular H-bond and with only a single 1,4-dioxane molecule at short distance.

occasionally in close vicinity of the solute as long as 100 ps before it is replaced by a more remote one. The jumps nearly always appear when an N12−H19 distance corresponding to an *intra*molecular H-bond is encountered. This reflects the competition between formation of an *intra*molecular H-bond and an *inter*molecular H-bond. There is a preference of H19 to form two H-bonds, either an *intra*molecular and an *inter*-molecular one or two *inter*molecular ones. The geometry which exists then, is shown in Figure 12.

Figure 13 shows the O18−H19 and N2−H19 distances as a function of time, obtained in the simulation of Z* in 1,4-dioxane with the condition of fixed charges. The H19− O18 distance reflects most of the time the existence of an *intra*molecular H-bond in Z*, which is temporarily destroyed for short periods of about 10 ps. Consistently, an N2−H19 distance of about the length of an H-bond, does not appear. Most of the time the configuration of Z* dwells in the energy well 2 of the FF potential energy surface shown in Figure 7b. In other words, Z* has been generated with an *intra*molecular H-bond, which is occasionally disrupted for periods as long as 10 ps, but which has a long average lifetime nevertheless. The period of rupture is long enough to allow a full rotation of the side group in Z*. However, no N2−H19 distance corresponding to an H-bond is then encountered. This means that the charge on N2 is insufficient for H-bond formation and therefore for the formation of K*.

When the site charges of Z* in 1,4-dioxane are allowed to vary with ϕ_1, the distances and dihedral angles depend on time

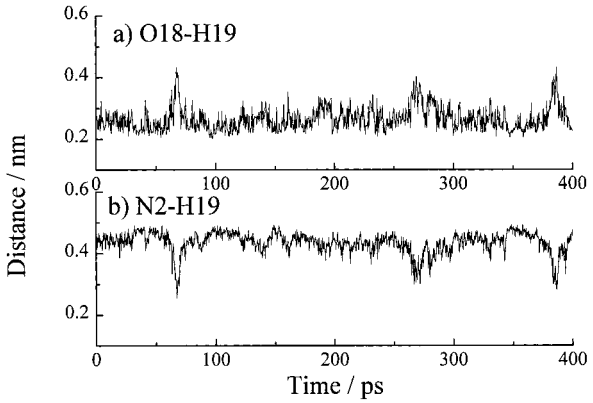

Figure 13. Time dependence of the O18−H19 and N2−H19 distances in the simulation of Z* in 1,4-dioxane with site charges in Z* kept fixed when ϕ_1 is varied.

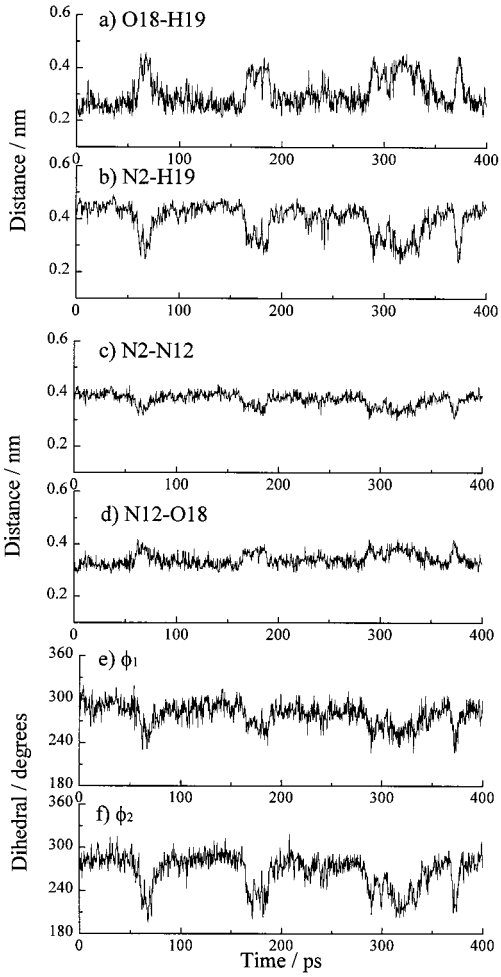

Figure 14. Time dependence of some distances and dihedral angles in the simulation of Z* in 1,4-dioxane with site charges in Z* varying as functions of ϕ_1.

as shown in Figure 14. These plots reveal clearly that a number of jumps in values of distances and dihedral angles are occurring simultaneously. This means that degrees of freedom are coupled. Under this condition an N2−H19 distance as short as the length of an H-bond frequently appears. The configuration of Z* with the H-bond between N2 and H19 corresponds to energy well 4 in the FF potential energy surface shown in Figure 7c. The observed formation of the N2−H19 hydrogen bond is crucial for the formation of K*, because only then is it possible to transfer H19 to N2 by tunneling. The proton H19 is carried by

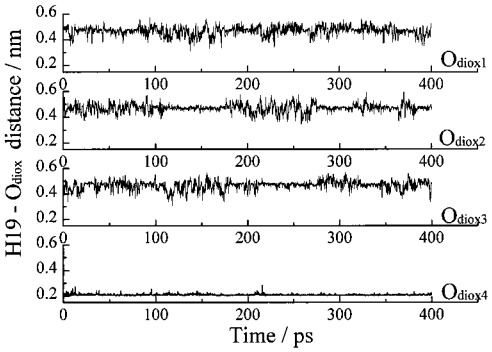

Figure 15. Time evolution of the H19−O_{diox} distance for the set of four nearest dioxane molecules around Z*.

the morpholino group from O18 to N2 in about 100 ps, which is five times shorter than the experimentally determined time for the conversion of Z* into K*. Apparently, the rotational motion of the side group is not damped sufficiently in the MD simulation. This is not surprising with regard to the simulated diffusion coefficients which are nearly three times larger than the experimental ones. Improvement may need a treatment which goes beyond the restriction of molecular pair interaction.

The evolution of the O_{diox}−H19 distance for the set of four nearest neighbors of Z* in liquid 1,4-dioxane can be revealed with the method applied in the case of E in 1,4-dioxane. The trajectories of the four nearest O_{diox} atoms are represented in Figure 15 by a plot of the O_{diox}−H19 distance as a function of time. This reveals that a single O_{diox} atom is found within an H-bond distance from H19, in contrast to the case of E where two such atoms are observed. The same O_{diox} remains H-bonded to H19 during the whole simulation period. This finding supports the experimentally based conclusion that a 1:1 complex between Z* and 1,4-dioxane[11,12] is formed. Two particular configurations of such a complex encountered in the simulation are shown in Figure 16. One configuration (a) has a short O18−H19 and a long N2−H19 distance and the other one (b) has a short N2−H19 and a long O18−H19 distance. Different start configurations of the simulation box have been chosen to see whether the complex formation depends on the initial conditions. It turns out that Z* appears as an H-bonded complex in all start configurations which satisfy the optimal conditions mentioned above for proton tunneling through the *intra*molecular H-bond in E. Simulations starting from configurations with the H19−N12 distance larger than 3 nm (i.e., no *intra*molecular H-bond) lead in the first stage to competition among O_{diox} atoms for H-bonding to H19 located in Z*. After these fluctuations, which last for about 1 ps, a persistent H-bonded complex is formed and from then on the same O_{diox} atom remains H-bonded to Z*.

When the system with Z* in cyclohexane is simulated with fixed charges, the initial H19−O18 distance of 0.22 nm is retained during the whole simulation (see Figure 17). In other words the *intra*molecular H-bond survives the whole simulation. Other distances and dihedral angles in Z* fluctuate with small amplitudes around their initial values. This means that the equilibrium structure of Z* does not change and corresponds to energy well 2 on the FF surface in Figure 7b. These results are not modified when the charges in Z* are allowed to change during the simulation. Although the equilibrium configuration of Z* does not correspond to the deepest potential well (Figure 7c), the *intra*molecular H-bond is retained and prevents the formation of K*. This is in accordance with the lack of any fluorescence arising from K* when HMMQ is dissolved in cyclohexane.

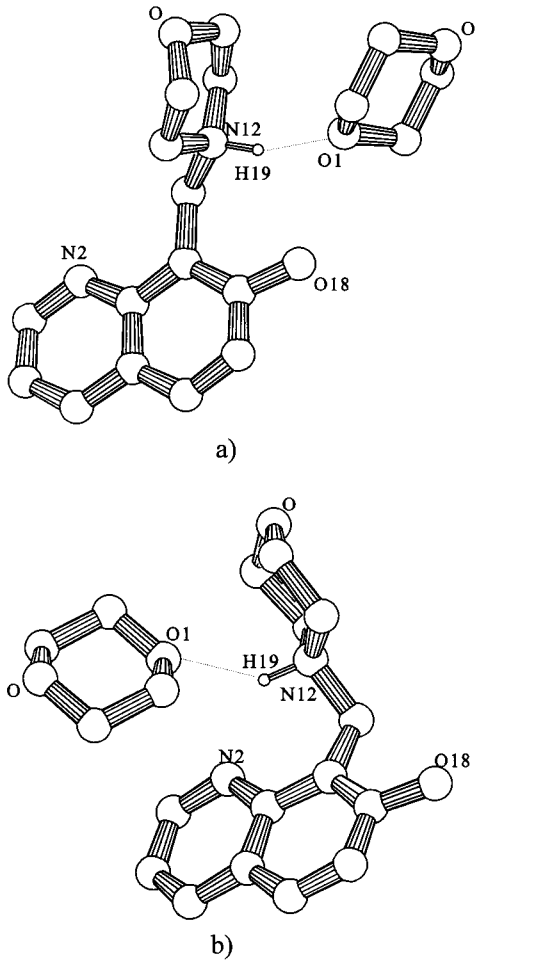

Figure 16. Configurations of the complex between Z* and a single 1,4-dioxane molecule; (a) with short O18−H19 distance; (b) with short N2−H19 distance.

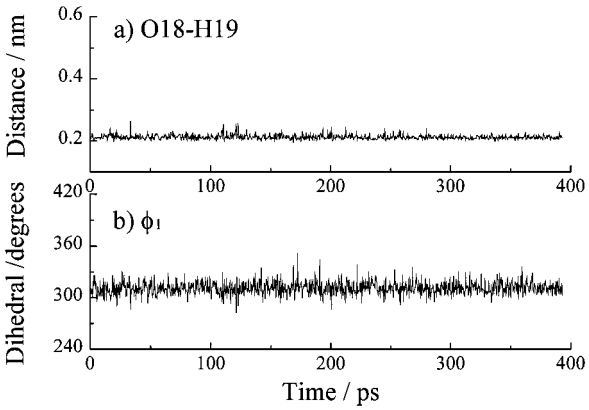

Figure 17. Time dependence of the O18−H19 distance and the angle ϕ_1 in the simulation of Z* in cyclohexane.

6. Concluding Remarks

Molecular dynamics simulations of the ground-state enol form of a single HMMQ molecule in either liquid cyclohexane or in liquid 1,4-dioxane reveal that the solute maintains an *intra*molecular H-bond in the former case, but that in the latter solvent it can have simultaneously both an *intra*molecular H-bond and an *inter*molecular H-bond with 1,4-dioxane or two *inter*molecular H-bonds involving the same proton and two 1,4-dioxane molecules (Figure 12).

Initially, the proton transferred from the OH group to the N atom in the morpholino group of Z* is maintaining an

*intra*molecular H-bond with its original binding site, but there is a small probability that this H-bond breaks. Then the protonated morpholino group turns out to be H-bonded to a 1,4-dioxane molecule, which it carries all along its path towards the N atom in the quinoline ring. Apparently, a 1,4-dioxane must have been within H-bonding distance relative to the proton position just before rupture of the initial *intra*molecular H-bond in Z*. This picture agrees with the conclusion from recent experimental work that the *intra*molecular H-bond in Z* breaks thermally only when the proton is also bound to a proton accepting solvent molecule.[34] When the site charges are allowed to vary during the rotation of the morpholino group, a stage (Figure 17) emerges in which an H-bond exists between the proton and the latter N atom, as required for delivery of the proton at its final site.

According to the simulation the time elapsed in the transition from the Z* form to the K* form in liquid 1,4-dioxane is five times shorter than experimentally observed. This is consistent with the fact that the diffusion coefficient of the solvent is also (three times) larger than the experimental one.

References and Notes

(1) Kramers, H. A. *Physica* **1940**, *7*, 284.

(2) Hänggi, P.; Talkner, P.; Borkovec, M. *Rev. Mod. Phys.* **1990**, *62*, 251.

(3) Tepper, E. L.; Pollak, E. *Chem. Br.* **1997**, *33*, 22.

(4) Brown, D.; Clark, H. R. *J. Chem. Phys.* **1990**, *92*, 3062.

(5) Edberg, R.; Evans, D. J.; Morris, G. P. *J. Chem. Phys.* **1987**, *87*, 5700.

(6) den Otter, W. K.; Briels, W. J. *J. Chem. Phys.* **1997**, *107*, 4968.

(7) Jalink, C. J.; Van Ingen, W. M.; Huizer, A. H.; Varma, C. A. G. O. *J. Chem. Soc., Faraday Trans.* **1991**, *87*, 1103.

(8) Jalink, C. J.; Huizer, A. H.; Varma, C. A. G. O. *J. Chem. Soc., Faraday Trans.* **1992**, *88*, 1643.

(9) Jalink, C. J.; Huizer, A. H.; Varma, C. A. G. O. *J. Chem. Soc., Faraday Trans.* **1992**, *88*, 2655.

(10) Jalink, C. J.; Huizer, A. H.; Varma, C. A. G. O. *J. Chem. Soc., Faraday Trans.* **1993**, *89*, 1677.

(11) Geerlings, J. D.; Huizer, A. H.; Varma, C. A. G. O. *J. Chem. Soc., Faraday Trans.* **1997**, *93*, 237.

(12) Geerlings, J. D.; Varma, C. A. G. O. *J. Photochem. Photobiol. A* **1999**, *129*, 129.

(13) Aqvist, J.; Warshel, A. *Chem. Rev.* **1993**, *93*, 2523.

(14) Truhlar, D. G.; Liu, Y. P.; Schenter, G. K.; Garrett, B. C. *J. Phys. Chem.* **1994**, *98*, 8396.

(15) Laria, D.; Ciccotti, G.; Ferrario, M.; Kapral, R. *J. Chem. Phys.* **1992**, *97*, 378.

(16) Borgis, D.; Hynes, J. T. *Chem. Phys.* **1993**, *170*, 315.

(17) Mavri, J.; Berendsen, H. J. C.; van Gunsteren, W. F. *J. Phys. Chem.* **1993**, *97*, 13 469.

(18) Mavri, J.; Berendsen, H. J. C. *J. Phys. Chem.* **1995**, *99*, 12 711.

(19) Staib, A.; Borgis, D.; Hynes, J. T. *J. Chem. Phys.* **1995**, *102*, 2487.

(20) Bala, P.; Grochowski, P.; Lesyng, B.; McCammon, J. A. *J. Phys. Chem.* **1996**, *100*, 2535.

(21) Hammes-Schiffer, S.; Tully, J. C. *J. Phys. Chem.* **1995**, *99*, 5793.

(22) Borgis, D.; Hynes, J. T. *J. Phys. Chem.* **1996**, *100*, 1118.

(23) Weiner, S. J.; Kollman, P. A.; Case, D. A.; Singh, U. C.; Ghio, C.; Alagona, G.; Profeta, S.; Weiner, P. *J. Am. Chem. Soc.* **1984**, *106*, 765.

(24) Weiner, S. J.; Kollman, P. A.; Nguyen, D. T.; Case, D. A. *J. Comput. Chem.* **1986**, *7*, 230.

(25) Van Gunsteren, W. F.; Berendsen, H. J. C. *Groningen Molecular Simulation Library*; Groningen, The Netherlands, 1987.

(26) Geerlings, J. D.; Varma, C. A. G. O.; van Hemert, M. C. *J. Phys. Chem. B* **2000**, *104*, 56.

(27) Guest, M. F.; Harrison, R. J.; Van Lenthe, J. H.; Van Corler, L. C. H. *Theor. Chim. Acta* **1987**, *71*, 117.

(28) Krestov, G. A. In *Thermodynamics of Solvation*; Burgess, J., Ed.; Ellis Harwood: New York, 1991.

(29) Pimentel, G. C.; McClellan, A. L. *The Hydrogen Bond*; Freeman: San Francisco, 1960; p 213.

(30) Ryckaert, J.: Ciccoti, G.; Berendsen, H. J. C. *J. Comput. Phys.* **1977**, *23*, 327.

(31) Berendsen, H. J. C.; Postma, J. P. M.; Van Gunsteren, W. F.; DiNola, A.; Haak, J. R. *J. Chem. Phys.* **1984**, *81*, 3684.

(32) Landolt-Börnstein, *Transport Phänomene I*; Springer: Berlin, 1969; p 592.

(33) Postma, J. P. M. Ph.D. Thesis, University of Groningen, Groningen, The Netherlands, p 100.

(34) de Bekker, E. J. A.; Geerlings, J. D.; Varma, C. A. G. O. *J. Phys. Chem. B* **2000**, *104*, scheduled for issue June.